Journal of Environmental Chemical Engineering 11 (2023) 109290

Contents lists available at ScienceDirect

Journal of Environmental Chemical Engineering

journal homepage: www.elsevier.com/locate/jece

Catalytic hydrolysis of cellulose to glucose: On the influence of graphene oxide morphology under microwave radiation

E. Frecha [a], D. Torres [a], J. Remón [a], R. Gammons [b], A.S. Matharu [b], I. Suelves [a], J.L. Pinilla [a,*]

[a] Instituto de Carboquímica, CSIC, C/ Miguel Luesma Castán 4, 50018 Zaragoza, Spain
[b] Green Chemistry Centre of Excellence, University of York, Department of Chemistry, Heslington, York YO10 5DD, UK

ARTICLE INFO

Keywords:
Graphene quantum dots
Graphene-oxide materials
Carbo-catalysts
Hydrolysis
Cellulose
Microwave absorbers

ABSTRACT

Carbon nanostructures provide a unique platform for the synthesis of novel catalysts for biomass conversion. In this work, a set of graphene oxide (GO)-based materials (nanofibers (GONF), sheets of few-layers (FLGO), and quantum dots (GOQD)), differing structurally in morphology and size, was prepared from fishbone-carbon nanofibers (CNF) and their catalytic behavior was compared on the hydrolysis of amorphous cellulose under microwave (MW) radiation. First, the influence of the reaction temperature (135–180 ºC), holding time (0–120 min), catalyst morphology and cellulose/water ratio (0.25–2.0 wt%) was thoroughly screened and compared with conventional heating mode. The use of GO morphologies in concert with MW energy showed the potential to achieve similar kinetic profiles than previously reported sulfonated carbons (110 kJ/mol) but using considerably less amount of catalyst (cellulose-to-catalyst ratio 12-fold lower). Overall, the reactivity of the GO-catalyst was related to their degree of oxidation/exfoliation, decreasing as follows: GOQD > FLGO > GONF. Compared with conventional heating, MW-technology enabled higher loadings of cellulose (2.0 *vs.* 0.25 wt%) to be processed in a shorter time (20 min instead of 24 h), which is a landmark achievement toward process intensification.

1. Introduction

Cellulose, an abundant natural polymer present in plant cell walls, is expected to be a key renewable feedstock for the transition from traditional fossil to bio-based industries [1–3]. The uniform and polyfunctional chemical composition of this carbohydrate, build-up from repeated units of glucose connected through β-1,4-glycosidic linkages, make it an attractive precursor for the synthesis of value-added products and fuel intermediates with minimal alteration on the parent material [4,5]. However, such simplicity at a molecular level belies a complex crystalline assembly, where an ubiquitous intra and inter-network of hydrogen bondings stabilize the structure, conferring it high resistance to transformations and water insolubility [6,7]. Hence, a critical step in the biorefinery schemes for cellulose valorization relies on the hydrolytic cleavage of all β-1,4-glycosidic linkages into simple sugars (hydrolysis reaction), which are the platforms for subsequent transformations [8,9]. Among many catalytic processes, acids and enzymes (cellulases) have been extensively considered for cellulose depolymerization [7,10]. The use of enzymes, although generally affords high glucose selectivity at mild temperatures, suffers from slow reaction rates that discourage their use at large scale, taking a few days to be completed. Also, their thermal denaturalization impairs the use of high temperatures to accelerate the reaction rate [11]. Instead, chemocatalytic methods have the potential to sort out these drawbacks. Mineral acids such as sulfuric (H_2SO_4), hydrochloric (HCl), nitric (HNO_3) or organic acids (oxalic, maleic, fumaric) have been successfully applied for the effective hydrolysis of cellulose at different concentrations and temperatures [4,12]. However, the use of homogeneous conditions always faces environmental and operational issues related to product separation, catalyst recycling and waste disposal. In this context, their replacement by heterogeneous systems in an aqueous phase is worth being considered, resonating with the ethos of green chemistry principles [7,13]. Nevertheless, designing solid catalysts for the effective depolymerization of cellulose remains a big challenge because it needs to overcome its robust architecture, excluding from the facile diffusion of the active sites of granular catalysts to inner ether linkages for their scissoring [14]. Many strategies have been explored in the last decades to cope with this physical barrier, including the use of mechanical pre-treatments to reduce the crystalline ordering and make the glucan chains more accessible [15–17] and/or the fine tuning of the

* Corresponding author.
E-mail address: jlpinilla@icb.csic.es (J.L. Pinilla).

https://doi.org/10.1016/j.jece.2023.109290
Received 14 September 2022; Received in revised form 9 December 2022; Accepted 6 January 2023
Available online 10 January 2023

catalyst properties [18].

Conceptually, a good solid catalyst for the hydrolysis of cellulose should bring strong acid sites, high affinity for the substrate (adsorption sites) and structural features compatible with the matrix bulkiness [6,19]. In this field, carbon nanostructures provide an ideal playground for catalyst engineering, with morphologies that range from three to zero-dimensionalities and surface moieties that can be incorporated through numerous functionalization approaches as per the reaction requirements [20–22]. Interestingly, the coexistence of various weakly acid polar groups onto the carbon surface, such as hydroxyl (-OH) and carboxylic species (-COOH), not only improve their water dispersion but also may serve as cellulose binders, allowing them to maximize the cut-off efficiency of catalytic sites with stronger Brönsted acidity such as sulfonic groups (-HSO_3), according to an enhanced-adsorption mechanism [23–25]. Equally important, the hydrophobic character of carbon materials may help to prevent the acid site deactivation in the aqueous medium, which often depletes in acidity by solvation [21]. In order to take fuller advantage of these functionalities, however, textural properties such as the pore size and surface area should be rationally considered [26]. A readily accessible arrangement between reactants and the active sites of a catalyst is depicted in membrane-like structures based on graphene oxide (GO) [27–29]. This morphology, described from a theoretical view point as planar sheets of one-atom thickness organized into a hexagonal crystal lattice, can be regarded as the ultimate model of a catalytic support, wherein all the surface functionalities become exposed [23,30]. Just on the limit of miniaturization of a heterogeneous catalyst, novel nanocarbons such as graphene quantum dots (GQD) could be similarly applied for biomass conversion reactions with promising prospects [31].

The interest in tailoring the graphene domain size at the nanometer scale goes beyond lessening mass transfer limitations. The type and number of surface chemical groups may be equally related to their structural dimensions. Thus, more edges are present as the sheet size decreases, which are the preferred sites for anchoring peripheral species such as carbonyl and carboxyl groups [32]. A higher density of edge-attached species would provide better dispersion in water and ease functionalization [33–35]. We recently reported the catalytic implications of gradually downscaling graphene oxide (GO) from bi- to zero-dimensional nanostructures with respect to cellulose hydrolysis [36]. F*ishbone* carbon nanofibers were used as the graphenic precursor of a set of GO derivatives, including nanofibers (GONF), sheets of few-layers (FLGO) and quantum dots (GOQD), and their hydrolytic activity was compared towards the conversion of amorphous cellulose at 135 ºC. The GOQD showed the highest glucose yield (60.1%), followed by GONF (50.7%) and FLGO (33.9%). This percentage rose to 83.5% when GOQD were co-milled with cellulose for 10 min (600 rpm), suggesting that the catalytic transformation was primarily governed by molecular collisions between the reactants [37]. In addition, long residence times (24 h) and mild conditions (135 ºC) had to be used in order to manage the delicate balance between the rate of hydrolysis of cellulose and sugar degradation. In this context, microwave (MW) technology could bring significant rewards in terms of reaction rate, glucose selectivity or solid contact efficiency [38–40]. A summary of recent research on MW-assisted hydrolysis of cellulose using carbon-based materials is shown in Table 1. For instance, Wu et al. studied the MW-assisted hydrolysis of microcrystalline cellulose catalyzed by a sulfonated biomass char (BC-SO_3H), noting a 3.8-fold higher yield of reducing sugars after 60 min at 90 ºC (16.7% of glucose and 7.4% of cello-oligosaccharides, Entry 1) than that obtained from conventional electric heating [40]. To illustrate the positive influence of MW irradiation on glucose selectivity, Sangib et al. compared the hydrolytic performance of a sulfonated bamboo-derived catalyst (SBC) under different heating means [41]. The maximum glucose yield (43.5%) was obtained at 180 °C upon 1 h of MW exposure (Entry 2). Similarly, Horikoshi *et al.* achieved 56% of glucose under MW-heating at 200 ºC for 30 min on a sulfonated activated carbon (AC-SO_3H, Entry 3) [42].

The origin of MW enhancement stems from a series of non-thermal effects, such as the suppression of wall effects or the sudden and selective heating of reaction components, according to their dielectric properties [45–47]. MW energy might also participate in the activation of cellulose throughout specific interactions [40,44,48,49]. At temperatures above 180 ºC, polar C-6 hydroxyl cellulose (CH_2OH) groups can experience localized rotations. Such changes in the spatial orientation may distort and open the H-bonded network, initiating the rupture of β-1,4-glycosidic bonds. The highest selectivity to glucose (75%) was achieved for a microcrystalline cellulose conversion of 14% after 1 min at 220 ºC [48].

Water as a solvent is also a good microwave absorber [50]. The dipolar motion of their molecules, trying to align with the electromagnetic field, creates friction which is dissipated into its surroundings as heat [38,43,51]. However, water tends to be MW-transparent with increasing temperature due to a loss of its dielectric properties [52–55]. This tendency impedes the use of high reaction temperatures, which is not only helpful in cellulose activation but also provides an environment rich in ionic species (H_3O^+) with acid utility [56,57]. To compensate for the drop in the dielectric constant of water, Mission *et al.* employed a reduced graphene oxide as a MW absorber. By this approach, a glucose yield of 66% was attained after 5 min at 241 ºC *vs.* 11.5% in the absence of a catalyst (Entry 4) [43]. To better understand this function, the adsorbing behavior of the catalyst should be considered. Carbon materials interact with MW energy by interfacial polarization, which is usually associated with micro-plasma formation (hotspots) and localized surface overheating [42,46,58,59]. The occurrence of high-temperature domains could amplify water dissociation nearby the catalyst, creating micro/nano environments with additional protonic sites active in the hydrolysis reaction [60].

In the previous example, most of the oxygen/sulfur entities were thermally detached from the catalyst surface through a MW-assisted hydrothermal treatment at 200 ºC and further annealing at 300 ºC.

Table 1
Catalytic results on the MW-assisted hydrolysis of cellulose using various carbon-based materials.

Substrate (S)	Catalyst (C)	S/C ratio	Temp. (ºC)	Time (min)	Conversion (%)	Glucose yield (wt%)	Ref.
Crystalline cellulose (13.3 wt%)	Sulfonated biomass (BC-SO_3H)	(2:1)	90	60	Nr	16.7	[40]
MCC (2.5 wt%)	Sulfonated Bamboo Carbon (SBC)	(1:1)	180	60	~60	43.5	[41]
MCC (0.25 wt%)	Sulfonated activated carbon (AC-SO_3H)	(1:1)	200	30	Nr	56.0	[42]
MCC (2 wt%)	Reduced graphene oxide (rGO)	(1:1)	240	5	78.3	65.5	[43]
MCC (2 wt%)	Graphite (Gr)	(1:1)	240	5	23.9	12.9	[43]
MCC (2 wt%)	Carbon nanotubes (CNF)	(1:1)	240	5	40.7	27.4	[43]
MCC (2 wt%)	Graphene oxide (GO)	(1:1)	180	60	Nr	61.0	[44]
Ball-milled cellulose (8 h, 600 rpm) (2.0 wt%)	GOQD	(1:1)	165	20	94.1	63.7	This work

MCC: microcrystalline cellulose
nd: not reported data.

This reduction stage restores the conjugated graphitic framework, which is essential for the electronic conduction and rapid heating of the system [43]. In fact, a greater degree of л-electron mobility on the graphenic network compared with other carbon nanostructures such as graphite (Gr) and multiwall nanotubes (CNT) might be behind their better outcome (12.9% of glucose from Gr and 27.4% from CNT, Entries 5,6). The synergistic effect between MW radiation and the functional groups of GO, mainly composed of oxygen and minor amounts of sulfur (0.6 wt %), was discussed in parallel by the same research group [44]. Apart from their intrinsic reactivity, the authors claimed that MW-absorbing features of these functionalities may find certain roles as molecular radiators, that is, species with high absorptivity that can be directly coupled with MW-energy to facilitate the heat transfer [61]. Yields of glucose as high as 61% were obtained after 60 min of exposure to MW at only 180 ºC (Entry 7) [44]. These promising results, likely among the best values reported thus far (Table 1), still leave room for a further level of control in the GO-surface features, such as the graphene domain size or the presence of sulfonic acid groups in quantitative proportions.

In this contribution, the cellulose to glucose hydrolytic potential of judiciously-designed GOQD under MW radiation is explored and compared with other paradigmatic structures of GO, such as sheets of few layers (FLGO) and graphene oxide nanofibers (GONF). Complementary, some reaction tests will be carried out under conventional heating, to establish a reliable comparison between traditional electric and microwave-assisted heating.

2. Experimental

2.1. Catalyst preparation

GONF, FLGO and GOQD were prepared by oxidative cutting of *fishbone* carbon nanofibers according to a modified Hummers method, followed by ultrasonic exfoliation and fractioning in size [62]. For this purpose, HNO_3-treated carbon nanofibers (CNF, 3.0 g) were oxidized by a mixture of $NaNO_3$ (3.0 g, Sigma Aldrich, purity ≥ 99.0%) and $KMnO_4$ (29.9 g, Panreac, 99%) in H_2SO_4 (126 mL, Panreac, 96%) under mild stirring. The reaction temperature was kept < 20 ºC during the addition of $KMnO_4$, hold at 30 ºC (± 5 ºC) for the next 2 h and at room temperature overnight. Ultra-pure water (240 mL) is then drop wised (<70 ºC) to the thick brown suspension and stirred for 1 h. Afterward, the mixture is diluted in another 600 mL of H_2O, reacted with H_2O_2 (29.9 mL, Panreac, 33%) to consume the excess of permanganate ions and sonicated for 1 h. The resulting material was finally recovered from the liquid solution by centrifugation (9500 rpm, 40 min), washed with a diluted hydrochloric acid solution (10% v/v, Panreac) thrice (9500, 40 min, 4 ºC) and fractioned in different products by means of a degressive differential centrifugation (DDC) sequence. This last process was minutely detailed elsewhere [36,62].

2.2. Catalyst characterization

The structure and chemical composition of catalysts were characterized by elemental analysis (EA), X-ray photoelectron spectroscopy (XPS), X-ray diffraction (XRD) and transmission electron microscopy (TEM). The quantitative determination of C, H, N and S was performed by EA (FlashEA® 1112 Analyzer, Thermo Scientific). Surface chemistry was studied by XPS (ESCAPlus OMICRON system) equipped with a hemispherical electron energy analyzer and a Mg K_α anode (λ = 1253.6 eV) as X-ray source. Binding energy values are referenced to the graphitic peak of the C 1 s core level (284.6 eV), using the Casa®XPS software for spectra processing. This signal includes the inherent contribution of adventitious carbon derived from the contamination of the apparatus itself. Powder XRD patterns were recorded in the θ-θ configuration (2θ=5º–80º, 0.05º/step, 4 s/step) with a Bruker instrument (Model D8 Advance, Series 2) and a Cu K_α anode (λ = 1.54 Å, 40.0 kV, 30.0 mA) with a secondary graphite monochromator. TEM images were taken with field emission scanning electron microscopy (Tecnai F30, FEI company) at 300 kV filament voltage, which allows a maximum point resolution of (1,5 Å). The samples were prepared by dropping the catalyst, previously suspended in water under ultrasound, onto carbon-coated 400-mesh copper grids.

2.3. Cellulose pretreatment

Prior to the reaction, the crystallinity of commercial cellulose (Fluka, Avicel® PH-101, particle size, 50 μm; microcrystalline-80%) was decreased by ball-milling. This was conducted in a planetary mill (PM 100 CM, Retsch, Germany) using ZrO_2 balls (Ø = 10 mm, n = 10) at a rotation speed of 10 Hz (600 rpm) for 8 h, including cool-down intervals of 10 min every 50 min of operation. Such conditions produced inherently pure amorphous cellulose (see details in [36]).

2.4. Hydrolysis tests

Hydrolysis tests were performed in a CEM Discover SP microwave reactor (CEM Corporation, Matthews, USA) with magnetic stirring and power control features. Experiments were run in dynamic mode, with a maximum power input of 40 W. In a typical run, an aqueous suspension (3 mL) containing the pre-treated cellulose (solid/water ratio = 0.25–2 wt%) and the catalyst (mass catalyst/cellulose ratio = 1:1) was first ultrasonically dispersed for 90 min inside a Pyrex glass vessel (10 mL). Afterward, it was microwave irradiated at a temperature between 135 and 180 ºC for a variable holding time (0–180 min). At the end of the reaction, the sample was air-chilled to 40 ºC and diluted with 10 mL of deionized water. The insoluble fraction, containing a mixture of the solid catalyst and unconsumed cellulose, was separated by vacuum filtration (glass microfiber, 0.22 μm, Whatman®), oven-dried (60 ºC) and weighed. The recovered solid residue was directly reused in a second run after supplementing some fresh cellulose in recycling tests. For comparison, several reactions were carried out using a conventional heating device (Berghof Products, BR-40 series, 45 mL), equipped with a temperature controller (BTC-3000) and a magnetic drive stirrer, following the same pre-/ and post-reaction methodologies.

2.5. Product analysis

The hydrolysate composition was analyzed by High-Performance Liquid Chromatography (Agilent 1260 Infinity HPLC apparatus), fitted with ultraviolet-visible (254 nm) and refractive index detectors and a Hi Plex H column (7.7 ×300 mm, particle size 8 μm, Agilent Technologies®, USA). The separation was achieved by isocratic elution of a volume sample (5 μL), using 0.6 mL/min of 5 mM H_2SO_4 as the mobile phase. The column and cell temperatures were held at 60 and 55 ºC, respectively. Routinely, the solution was re-filtered before the injection through a 0.45 μm PTFE syringe filter. The identity and quantification of products were based on the retention time and the calibration curves of commercial analytical standards.

For the analysis of samples prepared by conventional heating, a HPLC apparatus (Jasco model LC-2000 Plus Series) was used, provided with a semi-micro HPLC pump PU-2085, refractive index detector (Jasco RID-2031) and a ligand-exchange column (Reprogel Pb, 9 μm, 8 ×300 mm, ReproGel®, Maisch). The column, preceded by a guard column, was operated at 80 ºC using ultrapure H_2O (0.055 μS/cm) at a flow rate of 0.5 mL/min as eluent. Sample separation (injection volume of 50 μL) was completed within a run time of 56 min. Cell temperature was set to 30 ºC.

The product yields (Y) were calculated on a mass basis: Y (%) = (mass of product)/(mass of initial cellulose)× 100. The formation of high molecular mass polymeric compounds, including partially hydrolyzed oligosaccharides and humins, was determined through an indirect gravimetric method. To this end, 5 mL of the filtrate solution was oven-dried at 60 ºC to constant mass. The mismatch between this value

(accounting for the total of non-volatile substances) and the sum of chromatographic products above the water boiling point was ascribed to this type of macromolecular species. In this work, the conversion of cellulose (X) was defined taking into consideration water-soluble products only. It was expressed as the total soluble products with respect to the initial mass of cellulose: X (%) = (mass of products/mass of cellulose fed)× 100. Results were reproducible within a standard deviation of 4%.

The reaction rate was adjusted to a pseudo-first-order kinetic mechanism according to Eq. (1):

$$\frac{1}{m}\left(-\frac{dN}{dt}\right) = kN \tag{1}$$

$$\frac{1}{m}\frac{dX}{dt} = k(1-X) \tag{2}$$

with m, N, t and k being the mass of catalyst (g), cellulose amount (mol), reaction time (min) and kinetic constant for the pseudo-first-order reaction (min^{-1} g cat^{-1}), respectively. As it is difficult to define a mole of cellulose because its molecular weight varies, Eq. (2) shows the reaction rate defined using the cellulose conversion (X). This latter can be calculated as the amount (mol or mass) of cellulose converted with respect to the initial amount of cellulose (mol or mass) fed. This strategy avoids having to use mols to calculate the equation rate. The analytical solution in terms of cellulose conversion (X) of this differential equation fits a linear regression when the logarithm of 1/(1-X) is plotted against the reaction time (min), whose slope defines the value of the kinetic constant.

Variations of reaction rate with temperature follow the Arrhenius law. Thus, a linear relationship is obtained by plotting the logarithm of the k value (ln k) as a function of the reciprocal of the absolute temperature (1/T), whose slope and intercept denote the activation energy ($-E_a/R$) and pre-exponential factor ($\ln A_0$), respectively, Eq. (3):

$$k = A_0 \cdot e^{-\frac{E_a}{R\cdot T}} \tag{3}$$

3. Results and discussion

3.1. Physicochemical characterization of different GO-based catalysts

The treatment of CNF with $NaNO_3$, $KMnO_4$ and H_2SO_4 induced extensive oxidation of the parent graphitic material. The resulting material, denoted as graphene oxide nanofibers (GONF), reserves the filamentous structure of CNF but showing an expansion on the interlayer distance (0.81 *vs*. 0.34 nm) to accommodate the large variety of O- and S- functionalities. During this process, a portion of GONF de-laminated into a few layered-sheets (FLGO), which subsequently shrank into smaller domains based on graphene oxide quantum dots (GOQD). The three morphologies were size-separated, allowing access to a wide portfolio of GO-materials, each one presenting distinctive structural aspects and surface functionalities closely related to their size. The formation of these morphologies was duly reflected by X-Ray diffraction (Fig. 1). As briefly outlined above, the intercalation of multiple O- and S-containing groups onto the GONF is substantiated by the shift of (002) peak position of graphite (2θ=26.4°) to lower diffraction angles (2θ=10.8–11.2°), indicating an expanded lattice by oxidation. The progressive exfoliation gradually reduces the number of layers (n) and the crystal size (L_c), as shown in Fig. 1b. Such structural changes are additionally supported by the morphological appearance of each fraction as inspected by TEM (Fig. 2). The less exfoliated fraction (GONF), still retains the layered and filamentous structure of its parent CNF but showing a higher aspect ratio (width to length). A shortening in the fiber length results from a lower number of layers, reduced from 21.4 in CNF to 4.9 in GONF, with their planar sizes being 6.9 and 3.2 nm, respectively. The other two fractions are composed of smaller crystals, either organized into a lamellar film with folding properties (FLGO, Fig. 2b) or a more uniform membrane-like structure for GOQD (Fig. 2c). The latter is formed from an overlay of tiny sp^2-carbon domains, which is consistent with an almost featureless XRD pattern. In both cases, the transparency of FLGO and GOQD reflects a high exfoliation degree (n = 3.1 for FLGO and <2 for GOQD).

The surface chemical composition was individually assessed by XPS for each material (Fig. 3a). As seen from C 1 s XPS spectra, a variety of oxygen entities disrupt the carbon lattice, modifying the hybridization state from sp^2-planar to sp^3-tetrahedral. Apart from the C-S bond

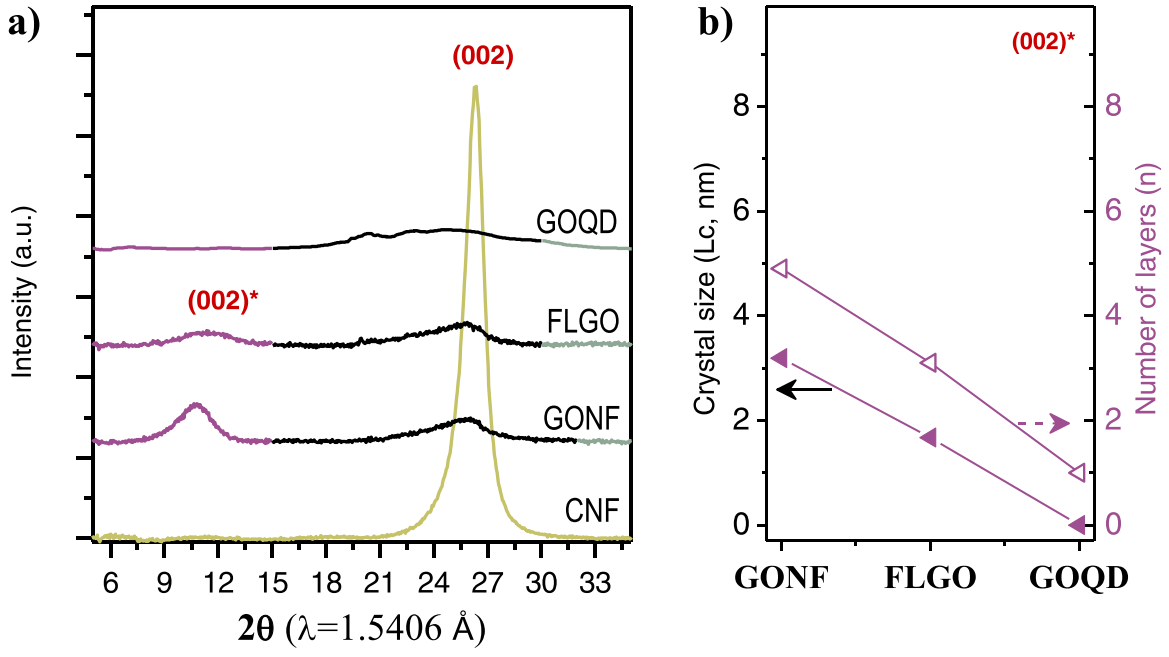

Fig. 1. XRD patterns of different GO-derivatives (a) and their structural parameters (number of layers; n and crystal size; L_C) determined from the (002)* peak (b).

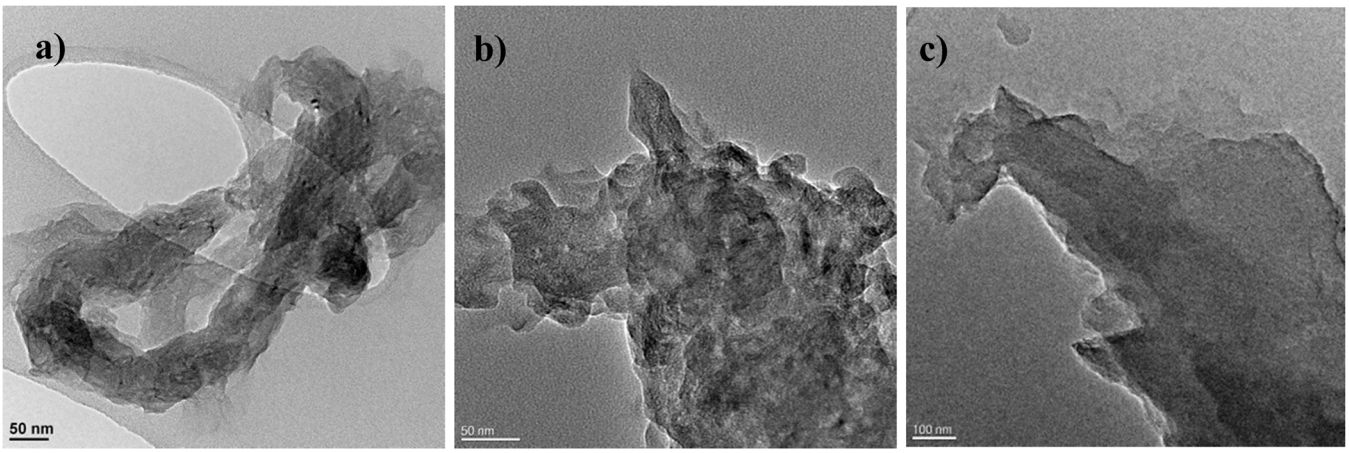

Fig. 2. TEM micrographs of GO-materials: a) GONF, b) FLGO and c) GOQD.

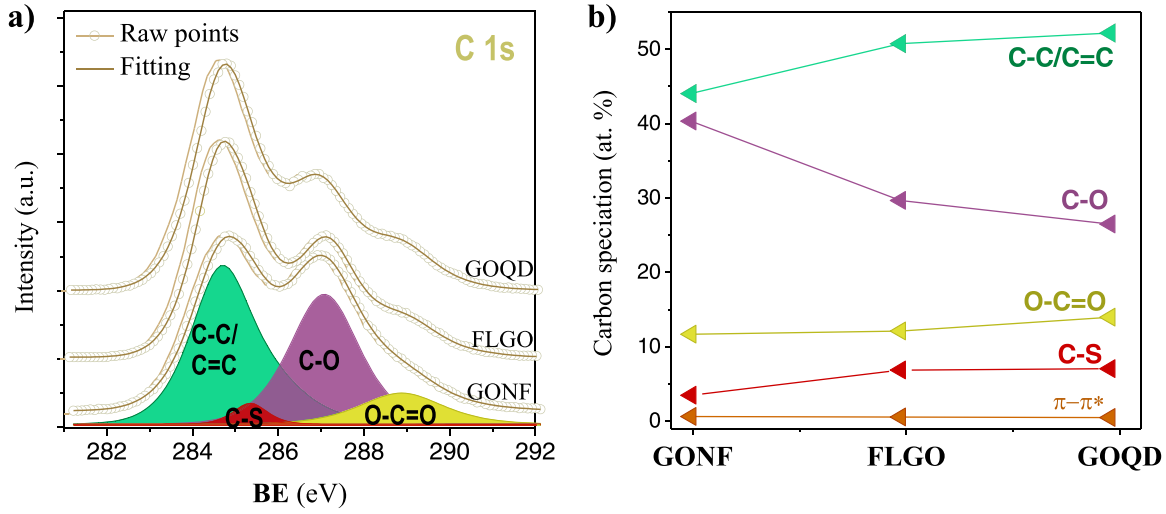

Fig. 3. C 1 s XPS analyses a) Spectra fitting for different fractions, b) carbon speciation.

(285.2 eV) and the almost indiscernible л-л* transition (291.0 eV), three main components can be distinguished from this photoemission region: i) an asymmetric peak at 284.6 eV combining aromatic and aliphatic carbon atoms (C═C/C-C), ii) oxygen-containing linkages such as C-O (286.5 eV) cognisant with hydroxyl and epoxides and iii) O-C═O (288.5 eV) of carbonyl/carboxylic groups. The relative proportion of different species varies with GO sheet size, thickness and layer structure, as plotted in Fig. 3b. As a general matter, the exfoliation process enhances the exposure of graphene planes, which gradually increases the surface carbon atomic percentage with respect to the bulk from GONF to FLGO and GOQD, whereas the л-л* shake-up feature vanishes with layers separation. On the other hand, smaller planar sizes enlarge the mean content of edge-functionalities (C═O) at the expense of the basal-plane species (C-O), alluding to the structural model described by Lerf-Klinowski [23,63,64]. Overall, the relative oxygen content remains higher over thinner fractions, ranging between 45.6%, 47.2% and 54.7%. Small percentages of sulfur were also anchored onto the carbon network, accounting for 1.92, 2.10 and 6.09 wt% of the bulk mass. From inspection of the 2p XPS spectra, it can be concluded that most of the S-compounds (> 95 at%) are present as sulfonic groups (-HSO_3, 168.4 eV, Fig. S1 in ESI).

3.2. Hydrolytic activity

3.2.1. Delimiting the operational intervals under different heating sources

MW dielectric heating obeys heating patterns (direct molecular activation, faster and selective) that are difficult to emulate by conventional means but often reduce the reaction timescales from hours to minutes [65]. Typically, up to 24 h are required for the hydrolysis of cellulose heated by conduction and convective currents. For example, we have previously identified the optimal conditions for glucose production from an aqueous suspension of amorphous cellulose (0.25 wt%) and using GOQD as a catalyst and a residence time of 24 h and 135 ºC as the operation temperature [36]. Over GONF, a glucose yield of 50.7% was attained at a conversion level of 70%. These conditions were used as the reference point for MW-heating tests but conducted at shorter periods of time (<120 min, Fig. 4). Only a modest conversion (21.3%) and negligible glucose yield (0.4%) were achieved in 60 min over GONF, which merely improved to 31.4% of conversion (5.55% of glucose yield) upon doubling the irradiation time (120 min). Cellulose conversion to glucose was markedly enhanced with increasing reaction time and temperature from 135 to 165 ºC, even when the time influence is less pronounced at 180 ºC. Both conversion and glucose yield increased monotonically from 20 to 120 min at 150 ºC and 165 ºC. After 120 min, 44.0% and 76.5% of the initial cellulose was converted at 150 and 165 ºC, yielding 23.7% (150 ºC) and 37.1% (165 °C) of glucose. On the contrary, an extension in the reaction time at 180 ºC had a minimal

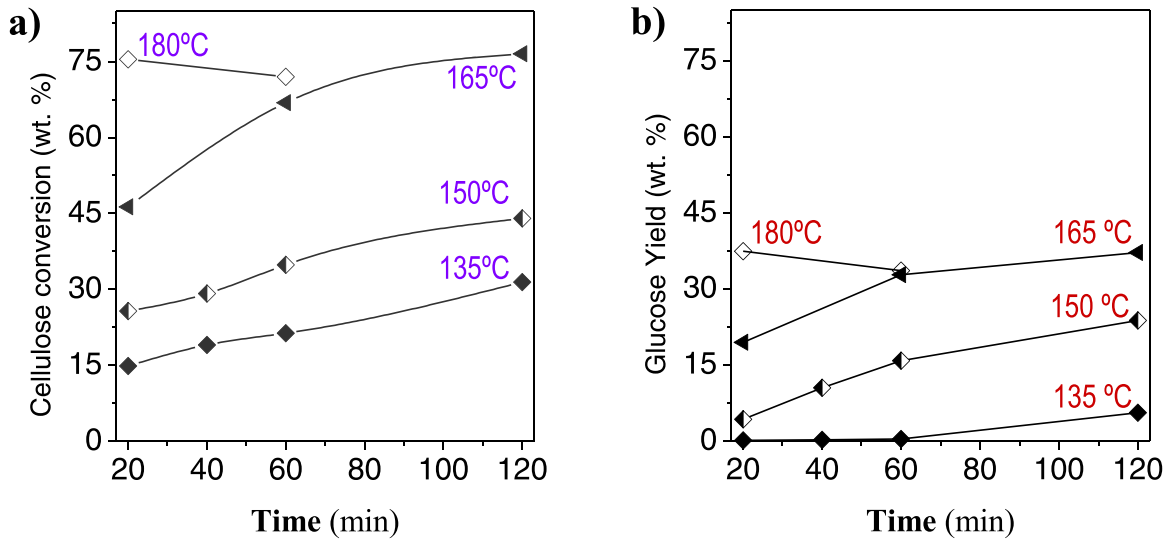

Fig. 4. Kinetic profiles of MW-assisted hydrolysis using a starting suspension of 0.25 wt% in cellulose and GONF as catalyst a) cellulose conversion and b) glucose yield.

effect on the glucose yield (37.4% and 33.4% after 20 and 60 min, respectively). A detailed analysis of other minor compounds present in the hydrolysate, including fructose, levoglucosan, levulinic and formic acids *inter alia,* is given in Table S1 (ESI). Overall, the formation of these products becomes apparent above 165 ºC at prolonged contact times (longer than 60 min) with a maximum weight of 10.4% at the most severe condition (*i.e.*, 180 ºC at a holding time of 60 min). The incipient degradation of sugars at elevated temperatures was the main reason for discontinuing the operation at 180 ºC, as it did not incur a better hydrolysis outcome.

Significant improvements in the hydrolysis activity were noted when GONF was replaced with GOQD as a catalyst, being invariably promoted for the overall set of reaction conditions (Fig. 5 and Table S2 in the ESI). The best result (52.1% glucose yield) was attained in 60 min at 165 ºC. The rich surface chemistry of GOQD, with no mass transfer limitations, may account for its better performance. Based on the characterization results, intermediate hydrolysis ability is expected for FLGO, a catalyst in the middle ground between the oxidation/exfoliation degree of GONF and GOQD. For that reason, this morphology was omitted from the first screening of variables.

Another important parameter controlling the hydrolysis rate relates to the cellulose-to-water ratio. In dilute suspensions, an excess of water may be absorbing the incident MW energy without meaningful participation in the reaction. MW radiation would instead be channeled toward the actual reacting molecules (*viz.*, catalyst and cellulose) when increasing their loadings in the system [44]. Such a conjecture was consistent with experimental results, where an increment in the cellulose-to-water ratio from 0.25 to 2 wt% rose the glucose yield 25-fold (from 0.1% to 10.2%) within 60 min at 135 ºC on GONF. This tendency was to some extent repeated irrespective of the catalyst morphology or the reaction temperature except for the GOQD at 165 ºC (Fig. 6a-b). At this point, a substantial amount of the glucose underwent successive degradation routes, driven by the acidic medium that results from the aqueous deprotonation of catalyst functionalities. On this basis, the usage of higher doses of GOQD, owning the highest density of surface groups, probably upsurges this effect.

Very differently, an increase in the cellulose-to-water ratio (2.0 wt%) was detrimental in conventional heating mode, dropping the glucose yield from 50.7% down to 31% in favor of recombination reactions of sugars to furan-based compounds (Table S3, Entries 2–3). The

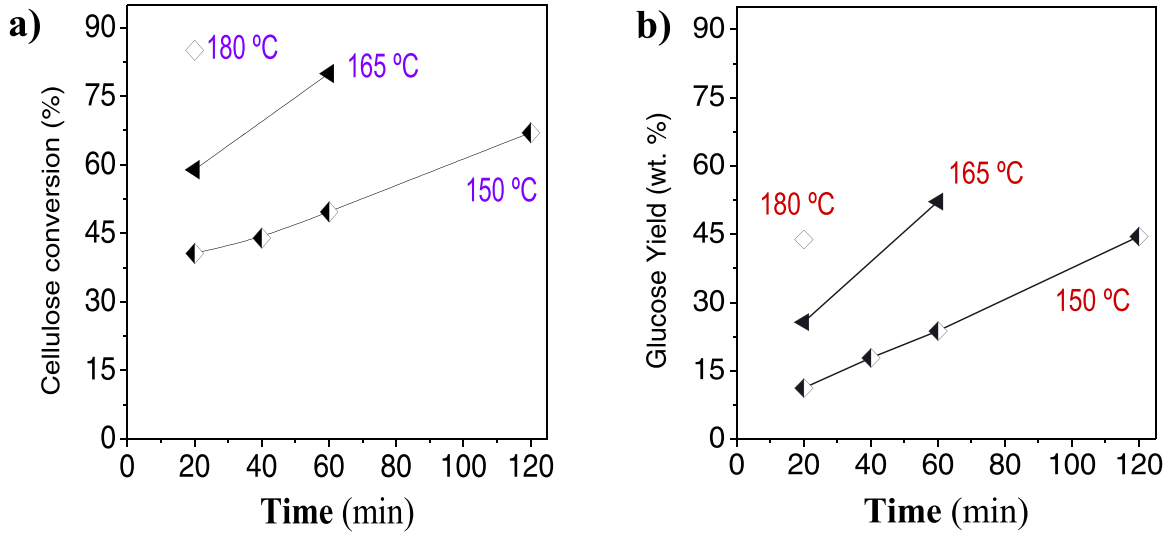

Fig. 5. Kinetic profiles of MW-assisted hydrolysis using a starting suspension of 0.25 wt% in cellulose and GOQD as catalyst a) cellulose conversion and b) glucose yield.

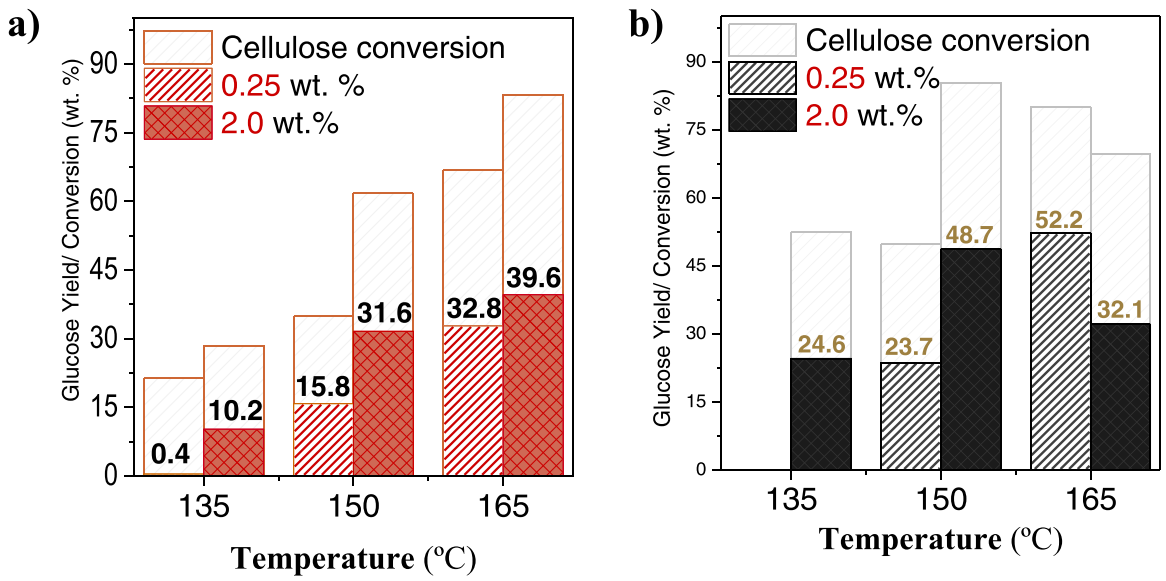

Fig. 6. Catalytic results as a function of the concentration of the initial suspension over GONF (a) and GOQD (b) as the catalysts (holding time of 60 min).

comparison was performed using GONF as a catalyst, keeping the rest of the conditions equal otherwise (24 h, 135 °C). A summary chart of the catalytic hydrolysis results from both heating sources is listed in Table 2. Essentially, it can be noted that whereas conventional heating requires mild conditions (135 °C) and high dilution ratios (0.25 wt% of cellulose), shorter time runs in MW-systems become compatible with higher temperatures (150–165 °C) and cellulose loadings (2.0 wt%).

3.3. *Effect of the GO morphology under MW-radiation*

In order to gain a more in depth comparison between different GO morphologies, a parametric optimization of the reaction was addressed over an initial cellulose suspension of 2 wt%. Fig. 7 displays the conversion of cellulose as a function of time for three temperatures (135, 150 and 165 °C) for each catalyst. As a rule of thumb, the order of reactivity of the GO-nanostructures followed the rank of their oxidation/exfoliation degree: GOQD > FLGO > GONF. However, the opposite behavior was observed at 165 °C from 40 min onwards due to the formation of insoluble by-products. Sugars degradation occurred to a greater extent over more acidic catalysts (GOQD), while it was much slower when less functionalized carbon materials (GONF) were employed. For a given GO-fraction, the hydrolysis rate was significantly promoted by raising the reaction temperature from 135 to 150 and 165 °C, as it was evidenced by the escalating conversion levels. Accordingly, the reaction time was shortened in 60 min for each step rise of 15 °C (180, 120 and 60 min at 135, 150 and 165 °C, respectively). Nonetheless, the vast majority of the reaction progress seemed to occur during the early stages but gradually leveled off. This observation is worthwhile to investigate in more detail in the future, as it could be a sign of the catalyst deactivation over time (*vide infra*). Besides, MW alone was unable to depolymerize cellulose at the relatively mild processing conditions applied in this study, as it was corroborated by non-catalytic experiments. In the absence of a catalyst, cellulose conversion was meager (6.61% after 120 min at 150 °C and 7.87% after 60 min at 165 °C), with no glucose determined (merely 0.2% at 165 °C).

The fate of dissolved cellulose was very time and temperature-dependent. The formation of sugars can be traced in Fig. 8, including glucose as the primary product (> 90 wt%) and minor quantities of cellobiose, fructose and levoglucosan (a dehydration product of glucose). Tables S4-6 list the specific distribution of products. Overall, the amount of compounds quantified by HPLC did not entirely account for the mass of liquid-phase products due to the presence of water-soluble cello-oligomers. The former suggests a stepwise mechanism, whereby cellulose is randomly broken down into shorter polymeric chains (cello-oligomers of varying lengths), which gradually decrease their degree of polymerization (DP) and finally produce the monosaccharide [66]. Sugars release evolved smoothly at 135 °C with negligible degradation over time (Fig. 8.a). The highest glucose yield (44.16%; 48.6% of sugars) was attained in 150 min in contact with GOQD. Under analogous conditions, the GO-morphologies based on FLGO and GONF afforded comparatively lower yields of glucose (36.6% and 32.5%, respectively), which did not upgrade when extending the irradiation time to 180 min. As cellulose conversion did, the production of sugars rose with increasing severity of conditions (150 and 165 °C), although not being stable in the reaction medium for a longer reaction times (Fig. 8.b-c). Thus, various stages can be distinguished from both

Table 2
Summary chart of catalytic hydrolysis results under different heating sources.

Catalyst	Heating source	Temp. (°C)	Time (h)	Initial loading 0.25 wt%		Initial loading 2.0 wt%	
				Cellulose conversion[a]	Glucose Yield	Cellulose conversion[a]	Glucose Yield
GONF	Conventional	135	24	70.0	50.7	53.9	33.8
		150	24	66.5	16.6	—	—
	MW	135	2	31.4	5.5	57.5	29.6
		150	1	34.9	15.8	61.8	37.1
GOQD	Conventional	135	24	83.9	60.1	—	—
	MW	150	1	49.7	23.7	79.7	50.2

[a]d)

Cellulose conversion was defined considering the formation of soluble products only.

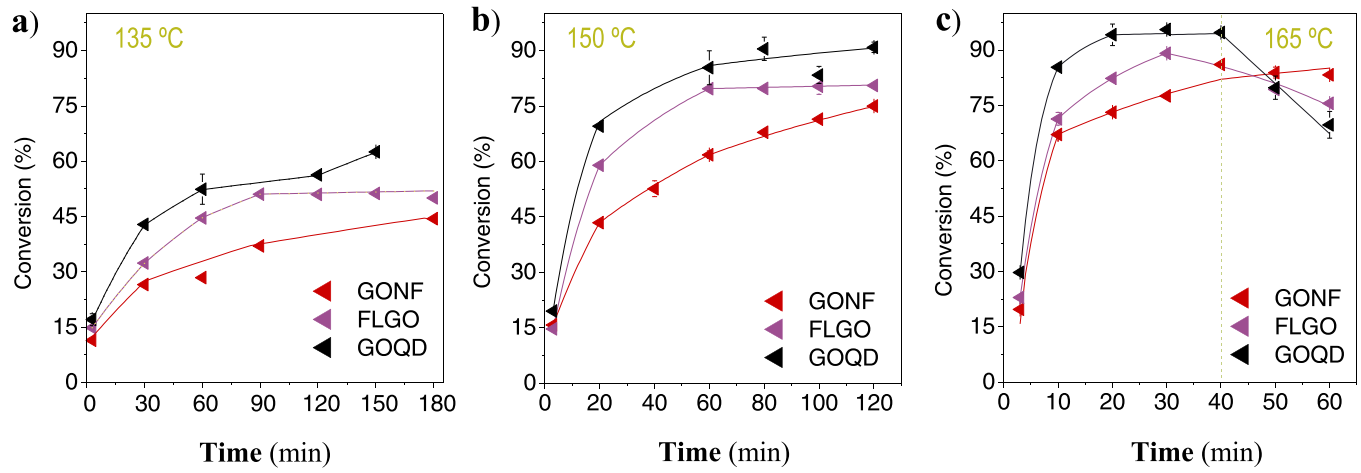

Fig. 7. Time-course of cellulose conversion in MW-assisted hydrolysis reaction on different GO-derivatives at several temperatures a) 135 °C, b) 150 °C and c) 165 °C. (Inlet solution= 2.0 wt% of cellulose).

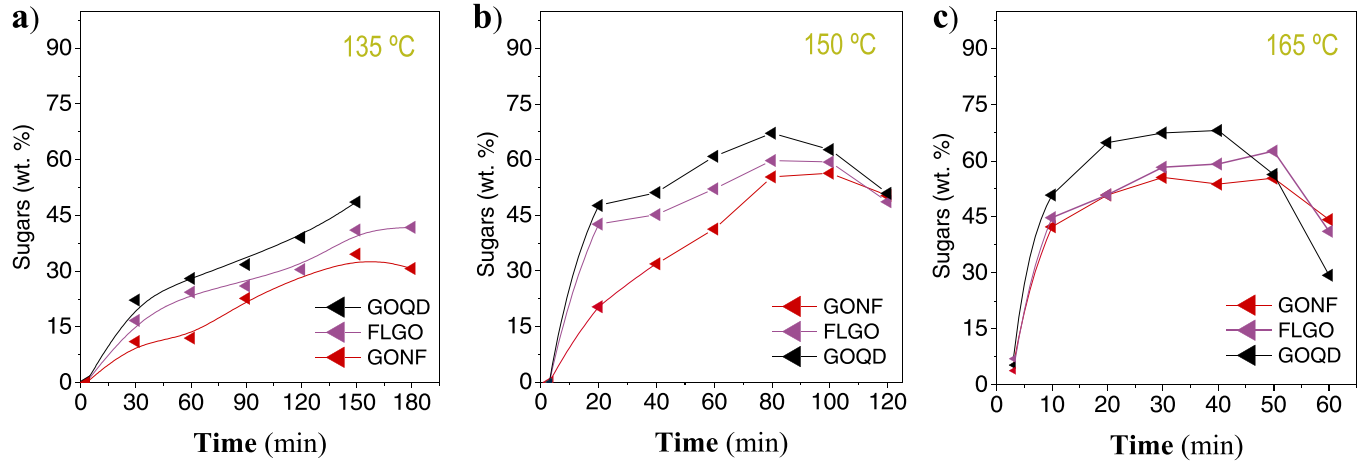

Fig. 8. Kinetic curves of production of sugars over different GO-morphologies at 135 °C (a), 150 °C (b) and 165 °C (c). (Inlet solution=2.0 wt% of cellulose).

time-resolved product profiles. In the beginning, glucose formation grew very fast. Thereupon, the reaction time loosely enhances the glucose accumulation but rather impacts its degradation. At 150 °C, the maximum glucose yield was determined within 80 min of reaction (62.1% with GOQD, 55.4% with FLGO and 48.9% with GONF), followed by a slight decline at a longer hydrolysis duration. An increment in the temperature to 165 °C intensified this profile; that is, glucose was rapidly produced in the initial stage until it reached a plateau at around 20 min (63.7% of glucose over GOQD). From 40 min onward, glucose was severely consumed by secondary side reactions. These diminishments are in line with the catalytic activity of the materials: GOQD > FLGO > GONF, suggesting that the catalysts also exert a significant influence on successive degradation routes, leading to glucose transformation into other species.

In particular, glucose depletion went on par with a steady increase in the levulinic acid yield (Fig. 9). This compound, accounting for up to 19.2% over GOQD, is the result of a series of acid-catalyzed transformations involving the isomerization of glucose into fructose and its further dehydration to 5-hydroxymethylfurfural (5-HMF). The subsequent aqueous-phase hydrolysis of 5-HMF produces levulinic and formic acids (Scheme 1). Most of these intermediate compounds, as well as several other by-products from glucose decomposition (organic acids such as acetic and formic or levoglucosan), were present in trace amounts in the liquid effluent. Afterward, poly-condensation reactions leading to humins were the major degradation pathways.

Zero-dimensional and highly oxygenated GOQD arise as a wisely designed structure for the hydrolysis of cellulose. In order to compare their reaction rate over other arrays of GO in a quantitative manner, the cellulose conversion profiles were used to determine the kinetic constant (k) and activation energy (E_a) for each catalyst. In a simplified approach, the hydrolysis reaction can be described by a pseudo-first-order kinetic model with respect to the cellulose amount [25,66–70] as stated in the experimental section. Table 3 compiles the resultant values for the whole set of reaction temperatures determined from the linear region, depicting the reaction rate for each temperature and 0.06 g of catalyst. Based on the correlation coefficient (R^2), experimental data can be adjusted to a pseudo-first-order kinetic model at the beginning of the reaction. However, this pattern is not maintained over time. There is a breakdown point upon which the reaction slows down and any catalytic activity is hard to discern. Even so, some worthy conclusions can still be outlined from these preliminary calculations. First of all, the kinetic constants gradually increased from GONF to FLGO and GOQD, although all values fall within the same order of magnitude. For the same GO morphology, the reaction rate augmented with every 15 °C rise in temperature. The interdependency of the reaction rate with temperature follows the Arrhenius law [25,69]. The Arrhenius parameters are summarized in Table 3. According to these estimations, it is possible to decrease the apparent activation energy from 172 kJ/mol down to 149 kJ/mol and 135 kJ/mol when gradually downsizing the catalyst morphology from GONF to FLGO and GOQD, which underscores the

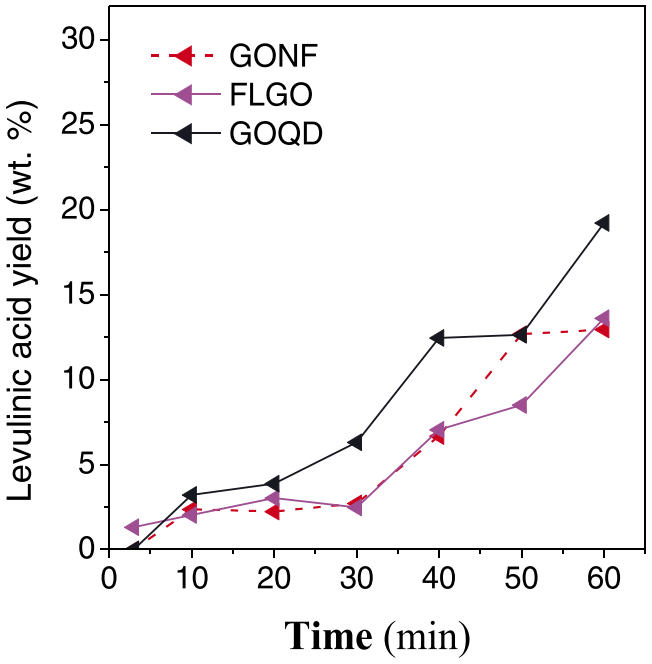

Fig. 9. Temporal evolution of levulinic acid at 165 ºC.

definite role of GOQD with respect to other GO nanostructures. Nonetheless, these values are only valid for the initial stage of the reaction, since all profiles meet after a certain point, upon which actual kinetic constants remain rather lower than those predicted from the data taken from the first interval. Taking as reference the catalytic activity of FLGO at 150 ºC, for example, the experimental data showed a gradual decay in the kinetic constant from 0.044 to 0.018 and 0.0008 min^{-1}, which further endorses the hypothesis of a lack of stability.

Besides, the macroscopic precipitation of the catalyst was observed from the outlet reactor stream for the overall set of experiments (Fig. S2, ESI). Worse dispersion properties may lead to an inefficient contact between reagents due to a loss on their large surface areas and explain its ulterior deactivation (Fig. S3). Likewise, some of the unique features of FLGO and GOQD adhered to their monolayer structure, and a more rich condition of surface functionalities could have been affected under MW radiation. This fact keeps the maximum glucose yield attained in our work (63.7%) at the same level as previous studies on the MW-assisted hydrolysis using GO (61% of glucose after 60 min at 180 ºC), declining expectations to overcome previous results through the GO-design.

In this sense, a possible solution against GO-restacking could be the use of co-solvent systems. For instance, Huang et *al.* proposed a mixture of water and *N*,*N*-dimethylacetamide (DMAc) in a volumetric ratio of 1:10 to preserve the individual layer morphology of a sulfonated graphene oxide. By this means, it was possible to retain around 93% of the original catalytic activity after five reaction cycles (8 h per cycle at 130 ºC). The addition of DMAc into the water also facilitated the cellulose solubilization to some extent [27]. In any case, if the catalyst reduction precedes the agglomeration, a re-oxidation stage could be required to regain the surface functionalities [71,72]. Work is in progress to address

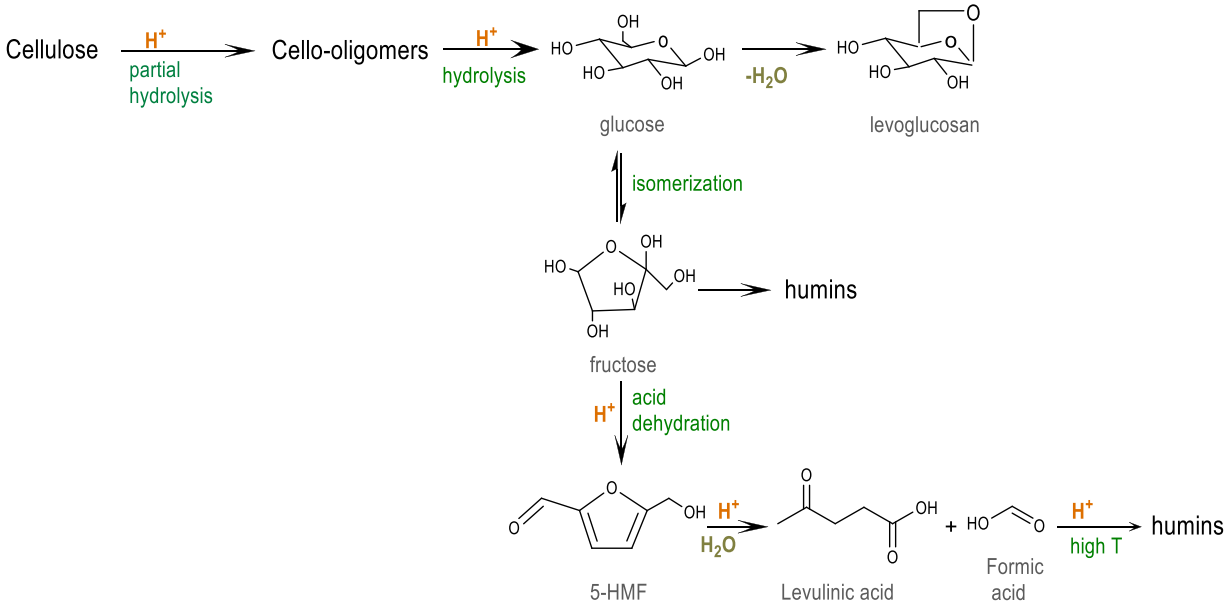

Scheme 1. Reactions network from cellulose to levulinic acid.

Table 3
Kinetic parameters for MW-assisted hydrolysis reaction at the beginning of the reaction.

Catalyst	$k_{135}^{[a]}$ (min^{-1})	R^2	$k_{150}^{[a]}$ (min^{-1})	R^2	$k_{165}^{[a]}$ (min^{-1})	R^2	lnA_0 (kJ/mol)	E_a (kJ/mol)
GONF	0.004 (0.060)	0.91	0.027 (0.447)	0.97	0.114 (1.905)	0.99	49.11	171.6
FLGO	0.006 (0.107)	0.98	0.044 (0.735)	0.99	0.128 (2.133)	0.99	43.05	148.9
GOQD	0.010 (0.162)	0.95	0.059 (0.980)	0.99	0.147 (2.453)	0.96	39.44	135.2

[a] Kinetic constants (min^{-1}) are for reaction rates over the amount of catalyst used in this work (0.06 g). Numbers in brackets denote the kinetic constants for any catalyst dosage ($min^{-1} \cdot g_{cat}^{-1}$).

the *ex-situ* regeneration of the catalyst and its further reutilization.

As a final remark, it is interesting to note that the kinetic parameters developed for the first interval favorably compare well with other E_a found in the literature for the acid hydrolysis of microcrystalline cellulose in conventional systems (170 kJ/mol in H_2SO_4) [25,69]. Moreover, the use of graphene oxide morphologies in concert with MW energy showed the potential to achieve similar kinetic profiles than previously reported sulfonated carbons (110 kJ/mol) but using considerably less amount of catalyst (cellulose-to-catalyst ratio 12-fold lower) [25]. For ease of comparison, the kinetic constant values per mass unit of catalyst ($min^{-1}{\cdot}g_{cat}^{-1}$) were included in brackets in Table 3. Additionally, a back-to-back comparison with the enzyme-catalyzed hydrolysis reveals that the activation energy of GO-morphologies remains much higher than that of cellulase (ranging between 13.3 and 26.2 kJ/mol depending on the source) [73,74]. Although a lower energy barrier allows operating at a milder temperature (50 ºC), the enzymatic reaction is often limited by cellulose feed concentrations to keep the presence of the reaction products (known as inhibitors) at low levels, which is another strong argument to opt for carbon-based materials instead of enzymes.

4. Conclusions

Seeking to harness the excellent dielectric properties of carbon materials, in tandem with the chemical reactivity of GO, this work examines the benefits of MW radiation on the GO-catalyzed hydrolysis of amorphous cellulose. Three different structures of GO, showing tailor-made dimensions and surface moieties that are specifically related to their size, were compared. MW technology emerges as a more time-effective heating route than conventional devices, decreasing the reaction time from typically 24 h to 20 min while the glucose yield is maintained. Nonetheless, the comparison between both heating methods is not straightforward and the operational variables should be redefined for each particular system. Under carefully controlled conditions, the maximum productivity of sugars (64.9%; 63.7% of glucose) was reached within 20 min at 165 ºC over GOQD. Generally, this morphology stands as the most active catalyst. The superior catalytic behavior of GOQD may be ascribed to various factors such as their excellent water dispersion, dimensionless structure and abundant surface moieties for adsorption, hydrolysis and MW-energy interaction. The most highlighted influence of the GO morphology was noted at the beginning of the reaction (first reaction minutes), with an activation energy that ranked in the following decreasing order: 171.6 kJ/mol (GONF) > 148.9 kJ/mol (FLGO) > 135.2 kJ/mol (GOQD). However, all GO morphologies underwent a gradual decay in their hydrolysis performance over time, which likely prevented better glucose production. It must be stressed, however, that MW reactors are capable of processing relatively high loadings of cellulose (2.0 wt%), other than quite diluted suspensions (0.25 wt%) required for conventional heating methods. That numerically means that one batch of MW-assisted hydrolysis produces the same amount of glucose as 8 hydrolysis cycles conducted at a traditional electric heating reactor.

CRediT authorship contribution statement

I. Suelves, J.L. Pinilla, J. Remón, A.S. Matharu: Conceptualization, Methodology. **E. Frecha, D. Torres, J. Remón, R. Gammons**: Validation, Investigation. **J.L. Pinilla, I. Suelves, A.S. Matharu**: Project administration, Funding acquisition. **I. Suelves, J.L. Pinilla, A.S. Matharu**: Supervision. **E. Frecha**: Writing – original draft. **J. Remón, D. Torres, I. Suelves, J.L. Pinilla, R. Gammons, A.S. Matharu**: Writing – review & editing. All authors contributed to manuscript revision, read, and approved the submitted version.

Declaration of Competing Interest

The authors declare that they have no known competing financial interests or personal relationships that could have appeared to influence the work reported in this paper.

Data availability

Data will be made available on request.

Acknowledgments

The authors are grateful for the financial support from the Spanish Ministry of Economy and Competitiveness (MINECO, Project ENE2017–83854-R) and the I+D+i project PID2020–115053RB-I00, funded by MCIN/ AEI/10.13039/501100011033. E.F. also thanks Ibercaja bank entity for a grant-in-aid for foreign research stays (CB 7/19). J.R. is grateful to the Spanish Ministry of Science, Innovation and Universities for the Juan de la Cierva Incorporación (JdC-I) fellowship (Grant Number: IJC2018–037110-I) awarded. DT is grateful for the Juan de la Cierva Incorporación (JdC-I) fellowship (Grant Number: IJC2020–045553-I) funded by MCIN/AEI/ 10.13039/501100011033 and by "European Union NextGenerationEU/PRTR".

Appendix A. Supporting information

Supplementary data associated with this article can be found in the online version at doi:10.1016/j.jece.2023.109290.

References

[1] I. Delidovich, K. Leonhard, R. Palkovits, Cellulose and hemicellulose valorisation: an integrated challenge of catalysis and reaction engineering, Energy Environ. Sci. 7 (9) (2014) 2803–2830.
[2] P. Bhaumik, P. Dhepe, Conversion of Biomass into Sugars, 2015, pp. 1–53.
[3] A. Cabiac, E. Guillon, F. Chambon, C. Pinel, F. Rataboul, N. Essayem, Cellulose reactivity and glycosidic bond cleavage in aqueous phase by catalytic and non catalytic transformations, Appl. Catal. A: Gen. 402 (1) (2011) 1–10.
[4] J. Verendel, T. Church, P. Andersson, Catalytic one-pot production of small organics from polysaccharides, Synthesis (2011) 1649–1677.
[5] J. Song, H. Fan, J. Ma, B. Han, Conversion of glucose and cellulose into value-added products in water and ionic liquids, Green. Chem. 15 (10) (2013) 2619–2635.
[6] J.A. Geboers, S. Van de Vyver, R. Ooms, B. Op de Beeck, P.A. Jacobs, B.F. Sels, Chemocatalytic conversion of cellulose: opportunities, advances and pitfalls, Catal. Sci. Technol. 1 (5) (2011) 714–726.
[7] L. Hu, L. Lin, Z. Wu, S. Zhou, S. Liu, Chemocatalytic hydrolysis of cellulose into glucose over solid acid catalysts, Appl. Catal. B: Environ. 174 175 (2015) 225–243.
[8] R. Rinaldi, F. Schueth, Acid hydrolysis of cellulose as the entry point into biorefinery schemes, ChemSusChem 2 (2009) 1096–1107.
[9] M.J. Climent, A. Corma, S. Iborra, Converting carbohydrates to bulk chemicals and fine chemicals over heterogeneous catalysts, Green. Chem. 13 (3) (2011) 520–540.
[10] R.D. Brown, L. Jurášek, P. Hydrolysis of Cellulose: Mechanisms of Enzymatic and Acid Catalysis, Advances in Chemistry, Vol. 181, American Chemical Society, 1979.
[11] G. Yang, X. Luo, L. Shuai, Bioinspired cellulase-mimetic solid acid catalysts for cellulose hydrolysis, Front. Bioeng. Biotechnol. 9 (2021).
[12] R. Palkovits, K. Tajvidi, J. Procelewska, R. Rinaldi, A. Ruppert, Hydrogenolysis of cellulose combining mineral acids and hydrogenation catalysts, Green. Chem. 12 (2010) 972–978.
[13] J. Matthiesen, T. Hoff, C. Liu, C. Pueschel, R. Rao, J.-P. Tessonnier, Functional carbons and carbon nanohybrids for the catalytic conversion of biomass to renewable chemicals in the condensed phase, Chin. J. Catal. 35 (6) (2014) 842–855.
[14] S. Van de Vyver, J. Geboers, L. Peng, F. Clippel, M. Dusselier, T. Vosch, L. Zhang, G. van Tendeloo, C. Gommes, B. Goderis, J. Pierre, B. Sels, Bridging the gap between cellulose chemistry and heterogeneous catalysis, Sustainable Chemistry 154 (2011) 129–140.
[15] Y. Liao, B.O. de Beeck, K. Thielemans, T. Ennaert, J. Snelders, M. Dusselier, C. M. Courtin, B.F. Sels, The role of pretreatment in the catalytic valorization of cellulose, Mol. Catal. 487 (2020), 110883.
[16] H. Kobayashi, M. Yabushita, T. Komanoya, K. Hara, I. Fujita, A. Fukuoka, High-yielding one-pot synthesis of glucose from cellulose using simple activated carbons and trace hydrochloric acid, ACS Catal. 3 (4) (2013) 581–587.
[17] Q. Zhang, M. Benoit, K. De Oliveira Vigier, J. Barrault, G. Jégou, M. Philippe, F. Jérôme, Pretreatment of microcrystalline cellulose by ultrasounds: effect of particle size in the heterogeneously-catalyzed hydrolysis of cellulose to glucose, Green. Chem. 15 (4) (2013) 963–969.
[18] R. Rinaldi, F. Schuth, Design of solid catalysts for the conversion of biomass, Energy 2 (2009) 610.

[19] A. Shrotri, H. Kobayashi, A. Fukuoka, Cellulose depolymerization over heterogeneous catalysts, Acc. Chem. Res. 51 (3) (2018) 761–768.
[20] CHAPTER 1 carbon (nano)materials for catalysis, Nanostructured Carbon Materials for Catalysis, The Royal Society of Chemistry,, 2015, pp. 1–45.
[21] F. Jérôme, S. Valange, Rational design of nanostructured carbon materials: contribution to cellulose processing, Nanotechnol. Catal. (2017) 627–654.
[22] C. Su, K.P. Loh, Carbocatalysts: graphene oxide and its derivatives, Acc. Chem. Res. 46 (10) (2013) 2275–2285.
[23] S. Zhu, J. Wang, W. Fan, Graphene-based catalysis for biomass conversion, Catal. Sci. Technol. 5 (8) (2015) 3845–3858.
[24] M. Kitano, D. Yamaguchi, S. Suganuma, K. Nakajima, H. Kato, S. Hayashi, M. Hara, Adsorption-enhanced hydrolysis of β-1,4-glucan on graphene-based amorphous carbon bearing SO3H, COOH, and OH Groups, Langmuir 25 (9) (2009) 5068–5075.
[25] S. Suganuma, K. Nakajima, M. Kitano, D. Yamaguchi, H. Kato, S. Hayashi, M. Hara, Hydrolysis of cellulose by amorphous carbon bearing SO3H, COOH, and OH groups, J. Am. Chem. Soc. 130 (38) (2008) 12787–12793.
[26] X. Zhao, J. Xu, A. Wang, T. Zhang, Porous carbon in catalytic transformation of cellulose, Cuihua Xuebao/Chin. J. Catal. 36 (2015) 1419–1427.
[27] L. Huang, H. Ye, S. Wang, Y. Li, Y. Zhang, W. Ma, W. Yu, Z. Zhou, Enhanced Hydrolysis of Cellulose by Highly Dispersed Sulfonated Graphene Oxide, BioResources 13 (2018).
[28] S. Stankovich, D.A. Dikin, G.H.B. Dommett, K.M. Kohlhaas, E.J. Zimney, E. A. Stach, R.D. Piner, S.T. Nguyen, R.S. Ruoff, Graphene-based composite materials, Nature 442 (7100) (2006) 282–286.
[29] S. Navalon, A. Dhakshinamoorthy, M. Alvaro, H. Garcia, Carbocatalysis by graphene-based materials, Chem. Rev. 114 (12) (2014) 6179–6212.
[30] V.K. Das, Z.B. Shifrina, L.M. Bronstein, Graphene and graphene-like materials in biomass conversion: paving the way to the future, Journal of Materials Chemistry A 5 (48) (2017) 25131–25143.
[31] K. Li, J. Chen, Y. Yan, Y. Min, H. Li, F. Xi, J. Liu, P. Chen, Quasi-homogeneous carbocatalysis for one-pot selective conversion of carbohydrates to 5-hydroxymethylfurfural using sulfonated graphene quantum dots, Carbon 136 (2018) 224–233.
[32] R. Yuge, M. Zhang, M. Tomonari, T. Yoshitake, S. Iijima, M. Yudasaka, Site Identification of Carboxyl Groups on Graphene Edges with Pt Derivatives, ACS Nano 2 (9) (2008) 1865–1870.
[33] D.R. Dreyer, S. Park, C.W. Bielawski, R.S. Ruoff, The chemistry of graphene oxide, Chem. Soc. Rev. 39 (1) (2010) 228–240.
[34] A.J. Paulista Neto, E.E. Fileti, Impact of edge groups on the hydration and aggregation properties of graphene oxide, J. Phys. Chem. B 122 (9) (2018) 2578–2586.
[35] Q. Wei, S. Pei, G. Wen, K. Huang, Z. Wu, Z. Liu, W. Ma, H.-M. Cheng, W. Ren, High yield controlled synthesis of nano-graphene oxide by water electrolytic oxidation of glassy carbon for metal-free catalysis, ACS Nano 13 (8) (2019) 9482–9490.
[36] E. Frecha, D. Torres, I. Suelves, J.L. Pinilla, Custom-sized graphene oxide for the hydrolysis of cellulose, Carbon 175 (2021) 429–439.
[37] M. Yabushita, H. Kobayashi, K. Hara, A. Fukuoka, Quantitative evaluation of ball-milling effects on the hydrolysis of cellulose catalysed by activated carbon, Catal. Sci. Technol. 4 (8) (2014) 2312–2317.
[38] A. Aguilar-Reynosa, A. Romaní, R. Ma. Rodríguez-Jasso, C.N. Aguilar, G. Garrote, H.A. Ruiz, Microwave heating processing as alternative of pretreatment in second-generation biorefinery: An overview, Energy Convers. Manag. 136 (2017) 50–65.
[39] G. Chatel, R. Varma, Ultrasound and microwave irradiation: contributions of alternate physicochemical activation methods to Green Chemistry, Green Chemistry 21 (2019).
[40] Y. Wu, Z. Fu, D. Yin, Q. Xu, F. Liu, C. Lu, L. Mao, Microwave-assisted hydrolysis of crystalline cellulose catalyzed by biomass char sulfonic acids, Green. Chem. 12 (4) (2010) 696–700.
[41] E.B. Sangib, B.T. Meshesha, B.A. Demessie, F. Medina, Study on cellulose (96% crystalline) hydrolysis performance of sulfonated carbon catalyst in microwave-heated reactor at elevated temperatures, Biomass Convers. Biorefinery 10 (4) (2020) 901–913.
[42] S. Horikoshi, T. Minagawa, S. Tsubaki, A. Onda, N. Serpone, Is Selective Heating of the Sulfonic Acid Catalyst AC-SO3H by Microwave Radiation Crucial in the Acid Hydrolysis of Cellulose to Glucose in Aqueous Media? Catalysts 7 (2017) 231.
[43] E.G. Mission, A.T. Quitain, Y. Hirano, M. Sasaki, M.J. Cocero, T. Kida, Integrating reduced graphene oxide with microwave-subcritical water for cellulose depolymerization, Catal. Sci. Technol. 8 (21) (2018) 5434–5444.
[44] E.G. Mission, A.T. Quitain, M. Sasaki, T. Kida, Synergizing graphene oxide with microwave irradiation for efficient cellulose depolymerization into glucose, Green. Chem. 19 (16) (2017) 3831–3843.
[45] A. Richel, P. Laurent, B. Wathelet, J.-P. Wathelet, M. Paquot, Current perspectives on microwave-enhanced reactions of monosaccharides promoted by heterogeneous catalysts, Catal. Today 167 (1) (2011) 141–147.
[46] A. de la Hoz, Á. Díaz-Ortiz, A. Moreno, Microwaves in organic synthesis. Thermal and non-thermal microwave effects, Chem. Soc. Rev. 34 (2) (2005) 164–178.
[47] M. Takahashi, H. Takenaka, DC electrical conductivity of cellulose, Polym. J. 15 (9) (1983) 625–629.
[48] J. Fan, M. De bruyn, V.L. Budarin, M.J. Gronnow, P.S. Shuttleworth, S. Breeden, D. J. Macquarrie, J.H. Clark, Direct microwave-assisted hydrothermal depolymerization of cellulose, J. Am. Chem. Soc. 135 (32) (2013) 11728–11731.
[49] V.L. Budarin, J.H. Clark, B.A. Lanigan, P. Shuttleworth, D.J. Macquarrie, Microwave assisted decomposition of cellulose: A new thermochemical route for biomass exploitation, Bioresour. Technol. 101 (10) (2010) 3776–3779.
[50] J. Wang, J. Xi, Y. Wang, Recent advances in the catalytic production of glucose from lignocellulosic biomass, Green. Chem. 17 (2) (2015) 737–751.
[51] M.R. Rosana, Y. Tao, A.E. Stiegman, G.B. Dudley, On the rational design of microwave-actuated organic reactions, Chem. Sci. 3 (4) (2012) 1240–1244.
[52] D. Cantero, M. Bermejo, M. Cocero, Pressure Effect on Cellulose Hydrolysis in Pressurized Water, 2013.
[53] I.K.M. Yu, X. Xiong, D.C.W. Tsang, Y.H. Ng, J.H. Clark, J. Fan, S. Zhang, C. Hu, Y. S. Ok, Graphite oxide- and graphene oxide-supported catalysts for microwave-assisted glucose isomerisation in water, Green. Chem. 21 (16) (2019) 4341–4353.
[54] M. Möller, F. Harnisch, U. Schröder, Microwave-assisted hydrothermal degradation of fructose and glucose in subcritical water, Biomass-.-. Bioenergy 39 (2012) 389–398.
[55] M. Möller, P. Nilges, F. Harnisch, U. Schröder, Subcritical Water as Reaction Environment: Fundamentals of Hydrothermal Biomass Transformation, ChemSusChem 4 (5) (2011) 566–579.
[56] F. Guo, Z. Fang, C.C. Xu, R.L. Smith, Solid acid mediated hydrolysis of biomass for producing biofuels, Prog. Energy Combust. Sci. 38 (5) (2012) 672–690.
[57] N. Akiya, P.E. Savage, Roles of water for chemical reactions in high-temperature water, Chem. Rev. 102 (8) (2002) 2725–2750.
[58] Microwave-assisted reactions on graphite, Microw. Org. Synth. (2002) 219–252.
[59] Microwave susceptors, Microw. Org. Synth. (2022) 297–346.
[60] E.G. Mission, J.K.C.N. Agutaya, A.T. Quitain, M. Sasaki, T. Kida, Carbocatalysed hydrolytic cleaving of the glycosidic bond in fucoidan under microwave irradiation, RSC Adv. 9 (52) (2019) 30325–30334.
[61] A.M. Rodríguez, P. Prieto, A. de la Hoz, A. Díaz-Ortiz, J.I. García, The issue of 'molecular radiators' in microwave-assisted reactions. Computational calculations on ring closing metathesis (RCM), Org. Biomol. Chem. 12 (15) (2014) 2436–2445.
[62] D. Torres, J.L. Pinilla, E.M. Gálvez, I. Suelves, Graphene quantum dots from fishbone carbon nanofibers, RSC Adv. 6 (54) (2016) 48504–48514.
[63] D.R. Dreyer, A.D. Todd, C.W. Bielawski, Harnessing the chemistry of graphene oxide, Chem. Soc. Rev. 43 (15) (2014) 5288–5301.
[64] A. Lerf, H. He, M. Forster, J. Klinowski, Structure of graphite oxide revisited, J. Phys. Chem. B 102 (23) (1998) 4477–4482.
[65] Z. Zhang, Z. Zhao, Solid acid and microwave-assisted hydrolysis of cellulose in ionic liquid, Carbohydr. Res. 344 (2009) 2069–2072.
[66] G.W. Huber, S. Iborra, A. Corma, Synthesis of transportation fuels from biomass: chemistry, catalysts, and engineering, Chem. Rev. 106 (9) (2006) 4044–4098.
[67] J.F. Saeman, Kinetics of wood saccharification - hydrolysis of cellulose and decomposition of sugars in dilute acid at high temperature, Ind. Eng. Chem. 37 (1) (1945) 43–52.
[68] J.S. Luterbacher, D. Martin Alonso, J.A. Dumesic, Targeted chemical upgrading of lignocellulosic biomass to platform molecules, Green. Chem. 16 (12) (2014) 4816–4838.
[69] L. Shuai, X. Pan, Hydrolysis of cellulose by cellulase-mimetic solid catalyst, Energy Environ. Sci. 5 (5) (2012) 6889–6894.
[70] H.-X. Li, X. Zhang, Q. Wang, D. Yang, Q. Cao, Le Jin, Study on the hydrolysis of cellulose with the regenerable and recyclable multifunctional solid acid as a catalyst and its catalytic hydrolytic kinetics, Cellulose 27 (2020).
[71] Y. Jiang, X. Li, X. Wang, L. Meng, H. Wang, G. Peng, X. Wang, X. Mu, Effective saccharification of lignocellulosic biomass over hydrolysis residue derived solid acid under microwave irradiation, Green. Chem. 14 (8) (2012) 2162–2167.
[72] X. Zhao, J. Wang, C. Chen, Y. Huang, A. Wang, T. Zhang, Graphene oxide for cellulose hydrolysis: how it works as a highly active catalyst? Chem. Commun. 50 (26) (2014) 3439–3442.
[73] M. Paljevac, M. Primožič, M. Habulin, Z. Novak, Ž. Knez, Hydrolysis of carboxymethyl cellulose catalyzed by cellulase immobilized on silica gels at low and high pressures, J. Supercrit. Fluids 43 (1) (2007) 74–80.
[74] Z. Xiao, P. Wang, Y. Qu, P. Gao, T. Wang, Cold adaptation of a mesophilic cellulase, EG III from Trichoderma reesei, by directed evolution, Sci. China Ser. C., Life Sci. 45 (4) (2002) 337–343.